

Towards the prediction of supersonic jet noise using a unified asymptotic approximation for the adjoint vector Green's function

M. Z. Afsar¹

Strathclyde University, Department of Mechanical & Aerospace Engineering, 75 Montrose St. Glasgow, G1 1XJ

A. Sescu²

Mississippi State University, Department of Aerospace Engineering, Starkville, MS 39762, USA

V. Sasanis³

Mississippi State University, Department of Aerospace Engineering, Starkville, MS 39762, USA

and

S. K. Lele⁴

Stanford University, Department of Mechanical Engineering, Palo Alto, CA 94305, USA

In this paper we continue efforts aimed at modeling jet noise using self-consistent analytical approaches within the generalized acoustic analogy (GAA) formulation. The GAA equations show that the far-field pressure fluctuation is given by a convolution product between a propagator tensor that depends on the (true) non-parallel jet mean flow and a generalized fluctuating stress tensor that is a stationary random function of time and includes the usual fluctuating Reynolds' stress tensor as well as enthalpy fluctuation components. Here, we focus on approximating the propagator tensor by determining an appropriate asymptotic solution to the adjoint vector Green's function that it depends on by using an asymptotic approach at all frequencies of interest for jet noise prediction. The Green's function is then rationally approximated by a composite formula in which the GSA (Goldstein-Sescu-Afsar, *J. Fluid Mech.*, vol. 695, pp. 199-234, 2012) non-parallel flow Green's function asymptotic solution is used at low frequencies and the $O(1)$ frequency parallel flow Green's function is used for all frequencies thereafter. The former solution uses the fact that non-parallelism will have a leading order effect on the Green's function everywhere in the jet under a distinguished scaling in which the jet spread rate is of the same order as the Strouhal number for a slowly-diverging mean flow expansion. Since this solution, however, is expected to apply up to the peak frequency, the latter $O(1)$ frequency Green's function in a parallel flow must be used at frequencies thereafter.

We investigate the predictive capability of the composite Green's function for the prediction of supersonic axi-symmetric round jets at fixed *jet* Mach number of 1.5 and two different temperature ratios (isothermal & heated) using Large-eddy simulation data. Our results show that, in the first instance, excellent jet noise predictions are obtained using the non-parallel flow asymptotic approach, remarkably, up to a Strouhal number of 0.5. This is true for both heated and un-heated jets. Furthermore, we develop the analytical approach required to extend this solution by appropriate asymptotic approximation to $O(1)$ frequencies.

Nomenclature:

c_∞	=	<i>ambient sound speed</i>
D_j	=	<i>nozzle diameter</i>
g	=	<i>Green's function</i>
I_w	=	<i>acoustic spectrum</i>
k	=	<i>turbulent kinetic energy</i>
k_1	=	<i>streamwise wavenumber</i>

¹ Member, AIAA.

² Assistant Professor, Senior member AIAA.

³ Member, AIAA.

⁴ Professor, Senior member AIAA.

l_i	=	<i>characteristic length scale</i>
M_a	=	<i>jet acoustic Mach number</i>
p	=	<i>pressure</i>
t	=	<i>time</i>
T	=	<i>averaging time</i>
U_c	=	<i>convection velocity</i>
V	=	<i>source volume</i>
\mathbf{v}_i	=	<i>velocity vector</i>
\mathbf{x}	=	<i>observer location</i>
\mathbf{y}	=	<i>source location</i>
γ	=	<i>specific heat ratio</i>
δ_{ij}	=	<i>Kronecker delta</i>
ε	=	<i>turbulence dissipation rate</i>
$\boldsymbol{\eta}$	=	<i>separation vector</i>
ρ	=	<i>density</i>
θ	=	<i>polar angle measured from jet axis</i>
τ	=	<i>time delay</i>
ω	=	<i>radian frequency</i>
∇	=	<i>gradient operator</i>
$ \bullet $	=	<i>absolute value</i>
<i>Subscripts</i>		
(i, j, k, l)	=	<i>tensor indices = (1,2,3)</i>
\perp	=	<i>transverse component</i>
<i>Superscripts</i>		
a	=	<i>adjoint</i>
$-$	=	<i>time average</i>
$'$	=	<i>fluctuating quantity</i>
\sim	=	<i>Favre average</i>
$*$	=	<i>complex conjugate</i>

I. Introduction

Ever since its inception in 2003, Goldstein's generalized acoustic analogy [2] has served as the most comprehensive and rational basis for modeling jet noise using an analogy approach of the type first invented by Lighthill [1] and in which the turbulence in the jet is assumed to be a known function that is modeled appropriately. The approach requires calculation of the adjoint vector Green's function of the linearized Euler equations for an, in general, non-parallel mean flow that is at $O(1)$ Mach numbers. This solution is then used to calculate the propagator tensor that enters the far-field acoustic spectrum formula as a convolution product with the auto-covariance tensor of a generalized stress tensor that is the assumed structure of the near field jet turbulence and which itself reduces to the fluctuating Reynolds stress in the absence of enthalpy fluctuations.

In this paper we use the Goldstein-Sescu-Afsar (2012) asymptotic theory [3] for the adjoint vector Green's function in non-parallel flows at low frequencies. The GSA theory showed that non-parallelism enters the leading order solution for the adjoint Green's function vector and therefore the propagator tensor when time variations are sufficiently slow in the sense that jet spread rate (which is taken to be an asymptotically small parameter) is the same order as the Strouhal number. This distinguished scaling gave the correct qualitative structure of the propagator when compared to the numerical solution of the full linearized Euler equations [3]. In

recent work, Afsar *et al.* [11] & [14] showed that the same theory, remarkably, provides excellent predictive capability for jet noise up to the peak frequency. In the latter study, the GSA theory (which was originally formulated for an isothermal jet flow) was extended to heated jets. The mean flow and turbulence statistics in that study was found using LES of two jets a fixed jet Mach number of 1.5 with different temperature ratios. The LES solutions were reported in Brès *et al.* 2012 & 2016 (refs. [12] & [13] respectively).

In this paper our aim is two fold: to summarize, in the first instance, the results obtained in Afsar *et al.* [14]. One should be aware of the importance of the results in that because (as opposed to the results in Afsar *et al.* [11]), it was found here that the asymptotic approach continues to provide excellent predictive capability up to a Strouhal number of 0.5 or 0.6, which is a region of frequency space thought to be more of $O(1)$ scale than asymptotically small values. Secondly, our aim is to develop the formalism to extend the Afsar *et al.* [14] analysis by including $O(1)$ frequency parallel flow Green's function (i.e. the solution to Rayleigh's equation), which will ultimately be part of a composite formula for the adjoint vector Green's function in which the GSA solution appears at low frequencies for only a single propagator (defined below) component that possesses the dipole-like acoustic efficiency that Goldstein first discovered in 1975 and which was subsequently re-discovered within the context of the GAA. The paper begins with a summary of the low frequency part of the composite Green's function formula (i.e. GSA theory) within the GAA equations followed by a short discussion of the Brès *et al.* test cases and the results obtained in Afsar *et al.* [14].

II. Composite formula for Adjoint Green's function vector

2.1 Summary of Goldstein's generalized acoustic analogy approach

The details here follow from Goldstein [2], G&L and GSA. Suppose that all lengths have been normalized by some characteristic nozzle radius, r_j , all velocities by the mean jet exit velocity U_j . Let the pressure p , density ρ , enthalpy h and speed of sound c satisfy the ideal gas law equation of state

$$p = \rho c^2 / \gamma, \quad h = c^2 / (\gamma - 1) \quad (1)$$

where γ denotes the specific heat ratio. The acoustic spectrum at the observation point $\mathbf{x} = \{x_1, x_2, x_3\}$ is given by Fourier transform

$$I_\omega(\mathbf{x}) \equiv \frac{1}{2\pi} \int_{-\infty}^{\infty} e^{i\omega\tau} \overline{p'(\mathbf{x}, t) p'(\mathbf{x}, t + \tau)} d\tau, \quad (2)$$

of the far-field pressure auto-covariance $\overline{p'(\mathbf{x}, t) p'(\mathbf{x}, t + \tau)}$. The acoustic spectrum at the far-field point, \mathbf{x} , due to a unit volume of turbulence at field point $\mathbf{y} = \{y_1, y_2, y_3\}$ in the jet is given by

$$I_\omega(\mathbf{x}) = \int_{V(\mathbf{y})} I_\omega(\mathbf{x} | \mathbf{y}) d\mathbf{y}, \quad (3)$$

where $V(\mathbf{y})$ is the entire source region, $p' \equiv p - \bar{p}$ and over-bars are being used to denote time averages. G & L showed that

$$I_\omega(\mathbf{x} | \mathbf{y}) = (2\pi)^2 \Gamma_{\lambda_j}(\mathbf{x} | \mathbf{y}; \omega) \int_{V(\mathbf{y})} \Gamma_{\kappa_l}^*(\mathbf{x} | \mathbf{y} + \boldsymbol{\eta}; \omega) \mathcal{A}_{\lambda_j \kappa_l}(\mathbf{y}, \boldsymbol{\eta}, \omega) d\boldsymbol{\eta} \quad (4)$$

Asterisks denote complex conjugate and the Einstein summation convention is being used with the Greek indices ranging from one to four and the Latin indices from one to three. The mean flow now enters the problem through the propagator

$$\Gamma_{\lambda_j}(\mathbf{y} | \mathbf{x}; \omega) \equiv \frac{\partial G_\lambda(\mathbf{y} | \mathbf{x}; \omega)}{\partial y_j} - (\gamma - 1) \delta_{\lambda k} \frac{\partial \tilde{v}_k}{\partial y_j} G_4(\mathbf{y} | \mathbf{x}; \omega) \quad (5)$$

that is a function of the Fourier transform

$$G_\lambda(\mathbf{y} | \mathbf{x}; \omega) \equiv \frac{1}{2\pi} \int_{-\infty}^{\infty} e^{i\omega(t-\tau)} g_{\lambda 4}^a(\mathbf{y}, \tau | \mathbf{x}, t) d(t - \tau), \quad \lambda=1,2,\dots,5 \quad (6)$$

of the 4th fourth component adjoint vector Green's function $g_{v_4}^a(\mathbf{y}, \tau | \mathbf{x}, t)$, $v = 1, 2, \dots, 5$ for the linearized Euler equations that appear on the left sides of the five generalized acoustic analogy equations (see Goldstein 2003 and equations (2.18)-(2.20) and equations (3.1)-(3.3) of G&L). Dowling et al (1978) show that the pressure-like adjoint Green's function, $g_{44}^a(\mathbf{y}, \tau | \mathbf{x}, t)$, possess incoming wave behavior at infinity in the (\mathbf{y}, τ) co-ordinates (since the adjoint Green's function corresponds to the usual direct Green's function in reverse time) and is weakly causal in time; i.e. decays at $\tau \rightarrow \infty$. Equations (4.8)-(4.10) of G&L show that the Fourier transformed vector Green's function, $G_\lambda(\mathbf{y} | \mathbf{x}; \omega)$, satisfies the adjoint equations

$$-\frac{\tilde{D}G_i}{D\tau} + G_j \frac{\partial \tilde{v}_j}{\partial y_i} - \tilde{c}^2 \frac{\partial G_4}{\partial y_i} + (\gamma - 1) X_i G_4 - \frac{\partial G_5}{\partial y_i} = 0 \quad (7)$$

$$-\frac{\tilde{D}G_4}{D\tau} - \frac{\partial G_i}{\partial y_i} + (\gamma - 1) G_4 \frac{\partial \tilde{v}_j}{\partial y_j} = \delta(\mathbf{x} - \mathbf{y}) \delta(t - \tau) \quad (8)$$

$$-\frac{\tilde{D}G_5}{D\tau} + X_i G_i = 0 \quad (9)$$

where the observation point \mathbf{x} is in the far field. Tilde denotes the Favre-average via usual relation, $\tilde{\bullet} \equiv \overline{(\rho \bullet)} / \bar{\rho}$ of any flow quantity; $v_k(\mathbf{y}, \tau)$ is the flow velocity and $\tilde{c}^2 \equiv \gamma \bar{p} / \bar{\rho}$ is the mean flow sound speed squared. The mean flow convective derivative is defined by $\tilde{D}/D\tau \equiv i\omega + \tilde{v}_i(\mathbf{y}) \partial / \partial y_i$ and $X_i \equiv \tilde{D}\tilde{v}_i / D\tau$ denotes the mean flow advection vector. Reciprocity theorem (Morse & Feshbach, p.873) shows that the dependent variable \mathbf{y} in $g_{v_4}^a(\mathbf{y}, \tau | \mathbf{x}, t)$ corresponds to the actual physical source point while \mathbf{x} corresponds to the observation location.

The tensor $\mathcal{R}_{\lambda_j \kappa l}$, -- for which suffixes $(i, j, k, l) = (1, 2, 3)$ and $(\lambda, \kappa) = (1, 2, 3, 4)$ -- in Eq. (4) is related to the Fourier transform

$$H_{\lambda_j \kappa l}(\mathbf{y}, \boldsymbol{\eta}, \omega) = \frac{1}{2\pi} \int_{-\infty}^{\infty} e^{-i\omega\tau} R_{\lambda_j \kappa l}(\mathbf{y}, \boldsymbol{\eta}, \tau) d\tau \quad (10)$$

of the generalized Reynolds stress auto-covariance tensor

$$R_{\lambda_j \kappa l}(\mathbf{y}, \boldsymbol{\eta}, \tau) \equiv \lim_{T \rightarrow \infty} \frac{1}{2T} \int_{-T}^T \left[\rho v'_\lambda v'_j - \overline{\rho v'_\lambda v'_j} \right](\mathbf{y}, \tau_0) \left[\rho v'_\kappa v'_l - \overline{\rho v'_\kappa v'_l} \right](\mathbf{y} + \boldsymbol{\eta}, \tau_0 + \tau) d\tau_0 \quad (11)$$

by the linear transformation $\mathcal{R}_{\lambda_j \kappa l} = \epsilon_{\lambda_j \sigma m} H_{\sigma m \gamma n} \epsilon_{\kappa l \gamma n}$ where $v'_\lambda \equiv v_\lambda - \tilde{v}_\lambda$ denotes a generalized, four-dimensional 'velocity' fluctuation, with $v_i = (v_1, v_2, v_3)$ being the ordinary fluid velocity and $v'_4(\mathbf{y}, \tau) \equiv (\gamma - 1)(h' + v'^2/2) = (c^2)'/2 + v'^2(\gamma - 1)/2$ where h' is the fluctuating enthalpy (G&L [4]). $(c^2)'$ denotes the fluctuation in the squared sound speed and $v'_4/(\gamma - 1)$ denotes the moving frame stagnation enthalpy fluctuation.

$\tilde{v}_k(\mathbf{y})$ denotes the steady Favre-averaged flow velocity and the tensor, $\boldsymbol{\varepsilon}_{\lambda j, \sigma m}$, is defined by outer product of appropriate unit tensors $\boldsymbol{\varepsilon}_{\lambda j, \sigma m} \equiv \delta_{\lambda \sigma} \delta_{j m} - \delta_{\lambda j} \delta_{\sigma m} (\gamma - 1)/2$.

The acoustic spectrum per unit volume is given by the general formula in Afsar *et al.* (2011) [8]:

$$I_\omega(\mathbf{x} | \mathbf{y}) = (2\pi)^2 \Gamma_{\lambda j}(\mathbf{x} | \mathbf{y}; \omega) \int_{V(\mathbf{y})} \Gamma_{\kappa l}^*(\mathbf{x} | \mathbf{y} + \boldsymbol{\eta}; \omega) \boldsymbol{\varepsilon}_{\lambda j \kappa l}(\mathbf{y}, \boldsymbol{\eta}, \omega) d\boldsymbol{\eta} . \quad (12)$$

It should be borne in mind that, Eqs. (4) & (5) are completely general and apply to any localized turbulent flow, even in the presence of fixed solid surfaces, say $S = S(\mathbf{y})$, as long as $g_{v_4}^a(\mathbf{y}, \boldsymbol{\tau} | \mathbf{x}, t)$ is assumed to satisfy $\hat{n}_i g_{i_4}^a(\mathbf{y}, \boldsymbol{\tau} | \mathbf{x}, t) = 0$ for \mathbf{y} on S where \hat{n}_i denotes the unit normal to $S(\mathbf{y})$.

Note also that since the dimensionless ratio, $v_4'/(|v_i'| U_j) = O(\sqrt{v_i'}/U_j)$ for cold jets (where $Ma = O(1)$) the enthalpy component $v_4'(\mathbf{y}, \boldsymbol{\tau})$ should, therefore, be small for cold jets and can be set to zero in $R_{\lambda j \kappa l}(\mathbf{y}, \boldsymbol{\eta}, \boldsymbol{\tau})$ which will equal zero whenever $(\lambda, \kappa) = 4$ (G&L, p. 307). In this paper, we consider the momentum transfer (i.e. non-heat related) components of $R_{\lambda j \kappa l}(\mathbf{y}, \boldsymbol{\eta}, \boldsymbol{\tau})$ only. The resulting acoustic spectrum formula simplifies to that given by G&L and Leib and Goldstein [10]. The propagator solution $\Gamma_{\lambda j}(\mathbf{x} | \mathbf{y}; \omega)$ will be found using matched asymptotic expansions as follows and, in particular, we analyze its '1-2' component.

2.2 Asymptotic structure of jet mean flow

Following G&L, GSA allow the (axi-symmetric) mean flow in the jet region to have small spread rate, say $\varepsilon \ll O(1)$, so that it varies on the slow streamwise length scale, $Y \equiv \varepsilon y_1$. In this case, it must expand as:

$$\tilde{\mathbf{v}}(\mathbf{y}) = \{U(Y, \mathbf{y}_T), \boldsymbol{\varepsilon} \mathbf{V}_T(Y, \mathbf{y}_T)\} + \varepsilon \{U^{(1)}(Y, \mathbf{y}_T), \boldsymbol{\varepsilon} \mathbf{V}_T^{(1)}(Y, \mathbf{y}_T)\} + \dots \quad (13)$$

$$\bar{\rho}(\mathbf{y}) = \bar{\rho}(Y, \mathbf{y}_T) + \varepsilon \bar{\rho}^{(1)}(Y, \mathbf{y}_T) + \dots, \quad (14)$$

$$\tilde{c}^2(\mathbf{y}) = \tilde{c}^2(Y, \mathbf{y}_T) + \varepsilon \tilde{c}^{2(1)}(Y, \mathbf{y}_T) \dots, \quad (15)$$

$$\bar{p}(\mathbf{y}) = \text{const.} + \varepsilon \bar{p}^{(1)}(Y, \mathbf{y}_T) + \dots \quad (16)$$

where the mean flow advection vector, X_i , commensurately, expands as

$$\mathbf{X}(\mathbf{y}) = \{\varepsilon \bar{X}_1, \varepsilon^2 \bar{X}_T\} + \varepsilon \{\varepsilon \bar{X}_1^{(1)}, \varepsilon^2 \bar{X}_T^{(1)}\} + \dots \quad (17)$$

The mean flow separates out into an inner region, given by Eqs. (13) --(17) for $r \equiv |\mathbf{y}_T| = \sqrt{y_2^2 + y_3^2} = O(1)$, and an outer region where the expansion break downs for $R \equiv \varepsilon r = O(1)$ for a cylindrical polar co-ordinate system $\mathbf{y}_T = (r, \Psi)$ with origin centered at the nozzle exit plane at the jet center-line and the observation point $\mathbf{x}_T = (R, \Psi)$ at a fixed point in the far-field relative to that plane.

2.3 Low frequency propagator solution for Strouhal numbers, $St \sim \varepsilon \ll O(1)$

GSA showed that non-parallel flow has an $O(1)$ effect on the solution to $G_\lambda(\mathbf{y}|\mathbf{x};\omega)$ everywhere in the flow at sufficiently low frequencies when time variations are of the same order as the streamwise variations in the mean flow, i.e. when $g_{v4}^a(\mathbf{y},\tau|\mathbf{x},t)$ depends on τ through $\tilde{T} \equiv \varepsilon\tau$ and at the distinguished frequency scaling when the Strouhal $St = fD_J/U_J$ number (based on jet diameter) is of the order of the jet spread rate, $St \sim \varepsilon$ in the solution to $G_\lambda(\mathbf{y}|\mathbf{x};\omega)$. The propagator solution is then defined at the particular scaled temporal frequency, $\Omega = \omega/\varepsilon = O(1)$ where $\varepsilon \ll O(1)$ is a small parameter. The asymptotic structure of the adjoint Green's function is then identical to the mean flow in that it also divides into an inner solution in the region where the radial distance $r = O(1)$ and into an outer solution in the region where $R = \varepsilon r = O(1)$. The richest inner equations are found by the non-trivial dominant balance of $g_{v4}^a(\mathbf{y},\tau|\mathbf{x},t)$ given by Eqs. 5.5 and 5.6 in GSA. The scaled Fourier transform of $g_{v4}^a(\mathbf{y},\tau|\mathbf{x},t)$ for $v = (1,4,5)$ then satisfies Eqs. (18)–(21) in Afsar *et al.* [11] for the leading order azimuthal mode expansion since higher order azimuthal modes produce an asymptotically small (i.e. $o(\varepsilon)$) correction to these inner equations. However, as shown in GSA, tremendous simplification can be achieved by taking (Y,U) as the independent variables of choice rather than (Y,r) . The implicit function theorem shows that $\mathbf{y} = (Y,r)$ can be implicitly related to the field space $\mathbf{y} = (Y,U(Y,r))$ and that the Green's function variable $G_i(\mathbf{y}|\mathbf{x};\Omega) = (G_1, G_4, G_5)(\mathbf{y}|\mathbf{x};\Omega)$ then depends on $(\mathbf{y};\Omega)$ through field space $(Y,U(Y,r);\Omega) \equiv (Y,r;\Omega)$. GSA showed that the one-to-one transformation of independent variables, $(Y,r) \rightarrow (Y,U)$, can be used together with the chain rule to combine the particular inner equations in to the second order hyperbolic PDE:

$$\tilde{c}^2 \frac{\partial}{\partial U} \left(\frac{1}{\tilde{c}^2} \bar{D}_0 \bar{v} \right) + \tilde{X}_1 \frac{\partial^2 \bar{v}}{\partial U^2} = 0 \quad (18)$$

in which $Y = \text{const.}$, $dU/dY = \tilde{X}_1/U$ are characteristic curves (Garebedian 1998, pp. 121-122). This equation requires that $\tilde{c}^2(Y,r) = f(U)$ and satisfies Crocco's relation [6] for the composite Green's function variable $\bar{v} \equiv \tilde{c}^2 \tilde{G}_4 + \tilde{G}_5$. But Afsar *et al.* [14] utilized the Crocco-Busemann relation (see Eq. 2.4c in Leeshafft *et al.* [7]), which applies when the jet flow is heated, and showed that the mean speed of sound is still a function of $U(Y,r)$. Therefore, Eq. (18) will continue to hold in such a case. The advantage of solving this equation to determine the low frequency structure of the adjoint linearized Euler equations (Eqs. 4.8 - 4.10 of G&L) is clear. The hyperbolic structure of Eq. (18) shows that it is unnecessary to impose a downstream boundary condition. Fig. 1 in GSA indicates how information propagates to both the left and the right from the $U = 0$ boundary and that no boundary conditions are required on the $Y = 0$ and $Y \rightarrow \infty$ boundaries (i.e. no inflow boundary condition is required here). Hence the solution for $\bar{v}(Y,U)$ is now uniquely determined by the outer boundary conditions (i.e. by matching to the inner limit of the outer solution using Van Dyke's rule),

$$\bar{v}(0,Y) \rightarrow -i\Omega c_\infty^2 e^{-i\Omega Y \cos\theta/c_\infty} \quad (19)$$

$$\frac{\partial \bar{v}}{\partial U}(0,Y) \rightarrow -i\Omega c_\infty \cos\theta e^{-i\Omega Y \cos\theta/c_\infty} \quad \text{with } Y \geq 0 \quad (20)$$

on the non-characteristic curve $U = 0$ (where, as indicated above, $U \rightarrow 0$ corresponds to $r \rightarrow \infty$). The coefficient $\tilde{X}_1 \equiv \tilde{D}U/D\tau$ is the Fourier transform streamwise component of the mean flow advection vector (Eq. 5.15 in GSA) and $\tilde{D}_0 \equiv i\Omega + U\partial/\partial Y$ in (18).

III. Mean flow structure of round jets at constant M_j and varying temperature ratio

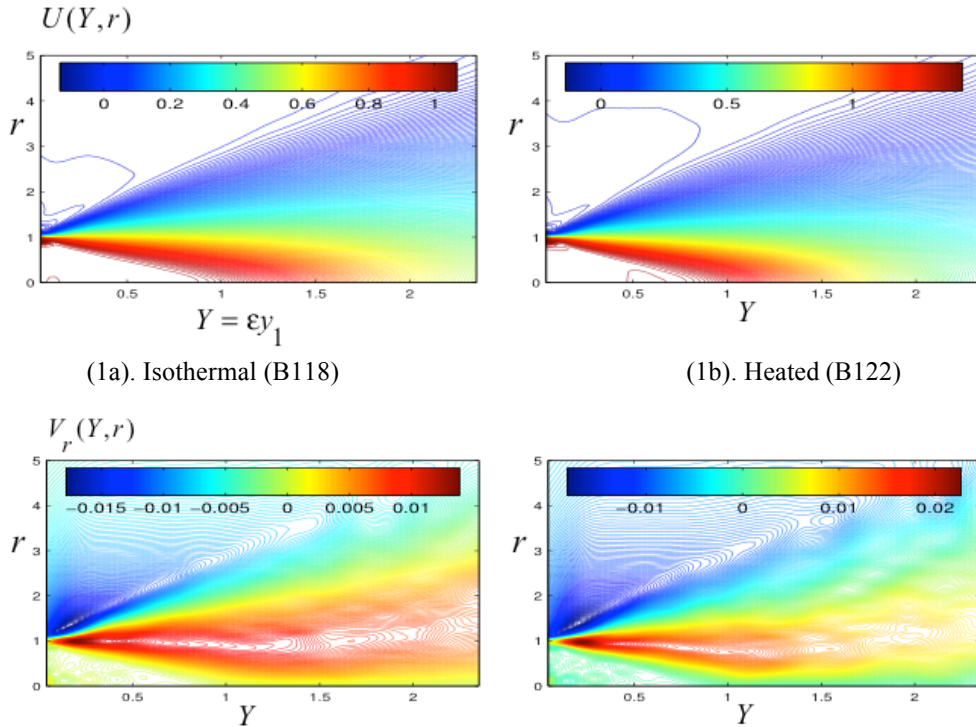
We consider the effect of heating and supersonic flow on the far-field noise using large-eddy simulations (LES) database of two axi-symmetric round jets at a fixed jet Mach number of, $M_j = 1.5$ within the GAA approach. These solutions were reported in Brès *et al.* [12] (see also Brès *et al.* [13]) and identified by the designations B118 & B122 for the unheated and heated configurations respectively. The operating conditions are summarized in table 1 below.

Experimental (Schlinker <i>et al.</i> (2012))	LES test case	Description	Jet Mach Number, M_j	Temperature ratio, TR	Acoustic Mach Number, Ma
B118	A1	Isothermal ideally-expanded	1.5	1.0	1.5
B122	A2	Heated ideally-expanded	1.5	1.74	1.98

Table 1. Brès *et al.* (2012) test cases

3.1 Mean flow

The spatial development of the streamwise component of the mean flow $U(Y, r)$, radial component of the mean flow $V_r(Y, r)$ and the advection component $\tilde{X}_1(Y, r)$ are shown in Figure 1, where the streamwise coordinate was scaled by the potential core length, and the radial coordinate by the nozzle radius. As expected, heating reduces the potential core length of the jet (Figs. 1a & 1b) as well as increasing the magnitude of $\tilde{X}_1(Y, r)$ along the shear layer of the jet (Figs. 1e & 1f).



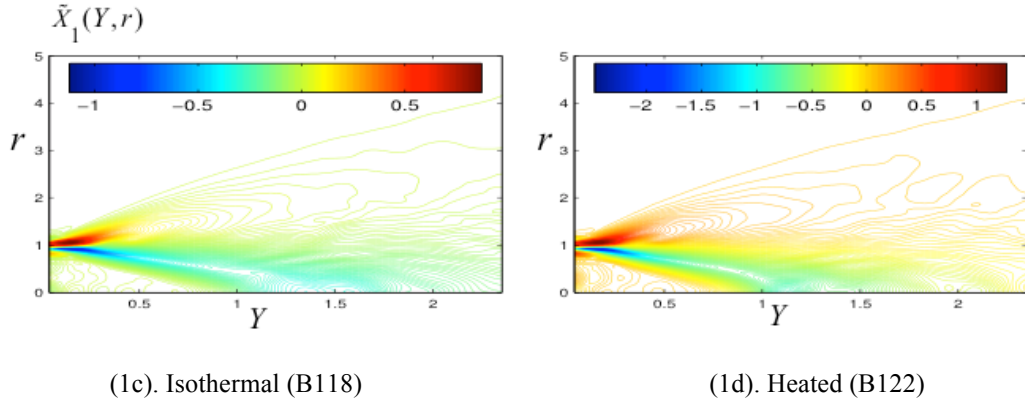


Figure 1. Streamwise component of mean flow. Spread rate = 0.12.

3.2 Turbulence structure for the peak radiated jet noise

Afsar *et al.* [11] showed that the $R_{1212}(y, \eta, \tau)$ component provides the maximum contribution to the peak jet noise at small observation angles to the jet axis. Figure 2 below shows its normalized structure with time delay τ at various streamwise spatial separations η_1 . The main indication of these results is that the heating of the jet appears to introduce little change in the decay of $R_{1212}(y, \eta, \tau)$ in the spatial location of importance for low frequency noise (i.e. $4 < y_1/D_J \leq 8$). Moreover, the anti-correlation of $R_{1212}(y, \eta, \tau)$, where the decay of $R_{1212}(y, \eta, \tau)$ is negative (commonly referred to as de-correlations or negative loops by various authors) is largely negligible in interval, $4 < y_1/D_J < 12$, and is therefore ignored in our mathematical model.

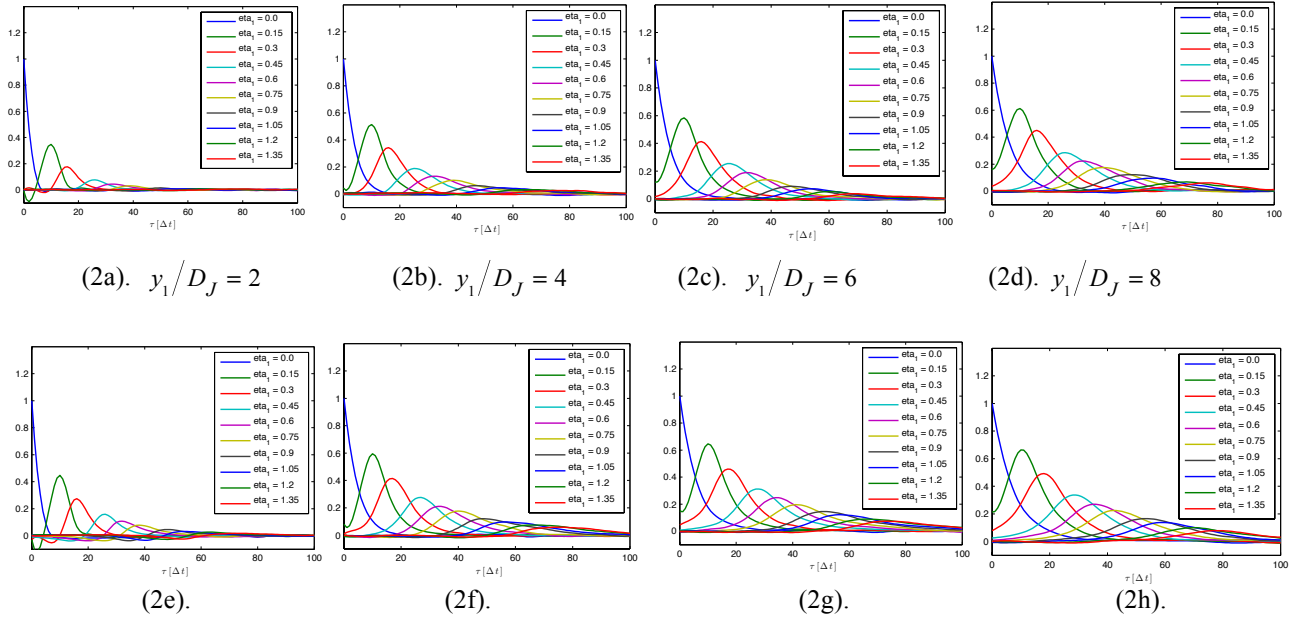


Figure 2. Normalized correlation function, $R_{1212}(y, \eta, \tau)$ along the shear layer. Top row is isothermal (B118) jet and bottom row is heated (B122).

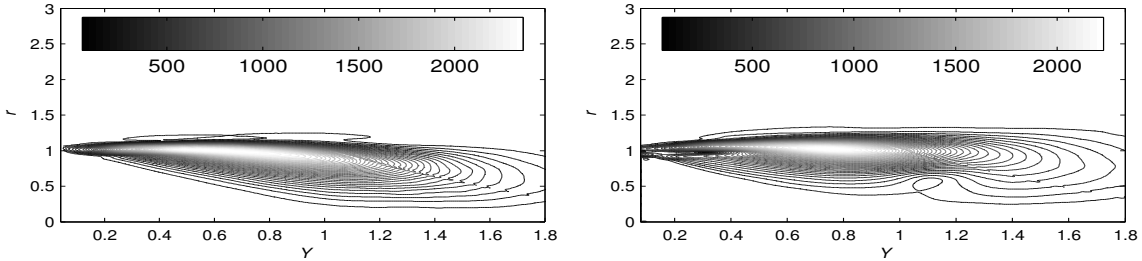
IV. Spatial structure of dominant propagator component & low frequency jet noise predictions

In Figs. 3a & b we show the noise predictions for B118 & B122 jets using a formula in which only the momentum transfer component $R_{1212}(\mathbf{y}, \boldsymbol{\eta}, \tau)$ of the generalized auto-covariance tensor $R_{\lambda j k l}(\mathbf{y}, \boldsymbol{\eta}, \tau)$ is retained. This component, as mentioned above, corresponds to the peak jet noise in an isothermal jet and is the first test of the present asymptotic formulation we perform preliminary calculations to assess whether this component alone can (with necessary tuning of the parameters) predict the heated jet noise spectrum. The acoustic spectrum formula is given by Eq. (38) in Afsar *et al.* [11],

$$I_{\omega}^{LOW}(\mathbf{x} | \mathbf{y}) \rightarrow \left(\frac{\varepsilon}{2c_{\infty}^2 |\mathbf{x}|} \right)^2 |\tilde{G}_{1r}(\mathbf{y}; \omega)|^2 \Phi_{1212}^*(\mathbf{y}, k_1, k_T^2, \omega) \quad \text{as } |\mathbf{x}| \rightarrow \infty. \quad (21)$$

It has been proved there (as well as in numerical computations in Karabasov *et al.* 2010) that the dominant propagator component is $|\tilde{G}_{1r}(\mathbf{y}; \omega)|$ where $\Phi_{1212}^*(\mathbf{y}, k_1, k_T^2, \omega)$ is the complex conjugate of the space-time Fourier transform of the fluctuating Reynolds stress auto-covariance tensor (11) with suffixes suitably contracted (see appendix A of [11]).

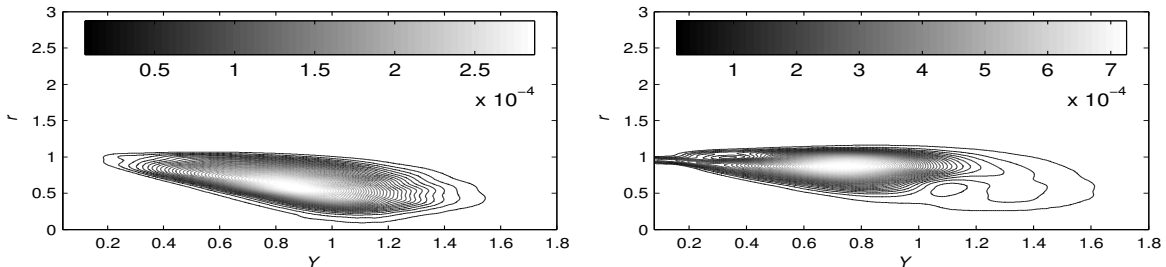
Figure 3 shows the contours of $|\tilde{G}_{1r}(\mathbf{y}; \omega)|$ at the peak frequency of $St = 0.2$ for B118 and B122 jets. The convergence of the numerical algorithm applied to inner equation (18) was analyzed in GSA and Afsar *et al.* (2016), and it was found to be within 5% at almost all regions of the jet, with only slight differences in results coming near the inner boundary as $U \rightarrow 1$. In Figures 4 (a,b) we show contour plots of the acoustic spectrum rI_{ω}^{LOW} . The indication here is that the peak noise source lies near $y_1 \sim 6$ (or $Y \sim 1$). The level of rI_{ω}^{LOW} is greater with heating (at fixed jet Mach number), which is consistent with the noise measurements of a heated flow at constant jet Mach number that shows an increase in sound of almost 10dB with temperature rise.



(3a). Isothermal (B118)

(3b). Heated (B122)

Figure 3. Contours of $|\tilde{G}_{1r}(\mathbf{y}; \omega)|$ at peak Strouhal number = 0.2.



(4a). Isothermal (B118)

(4b). Heated (B122)

Figure 4. Contours of $rI_{\omega}^{LOW}(\mathbf{x} | \mathbf{y})$ at peak Strouhal number = 0.2.

The results below show, remarkably, that the predictions remain in close agreement with the data upto a Strouhal number of 0.6 for the isothermal jet (Fig. 3a). Moreover, with heating, the predictions are equally as accurate. The parameters associated with the streamwise space and time decay of $R_{1212}(y, \eta, \tau)$ have been kept the same (which is justified given the similarity shown in Figs. 2a & 2b) in both predictions. However, any predictions in the heated jet case must be interpreted as a first approximation since Eq. (38) in Afsar *et al.* [11] does not include auto-variances and co-variances associated with enthalpy flux and momentum flux/enthalpy flux coupling respectively. Indeed it is true that the ‘low frequency’ sound region of these jets is elongated and much more broad band than the subsonic regime. However, the robustness of the asymptotic approach we have used here is clear.

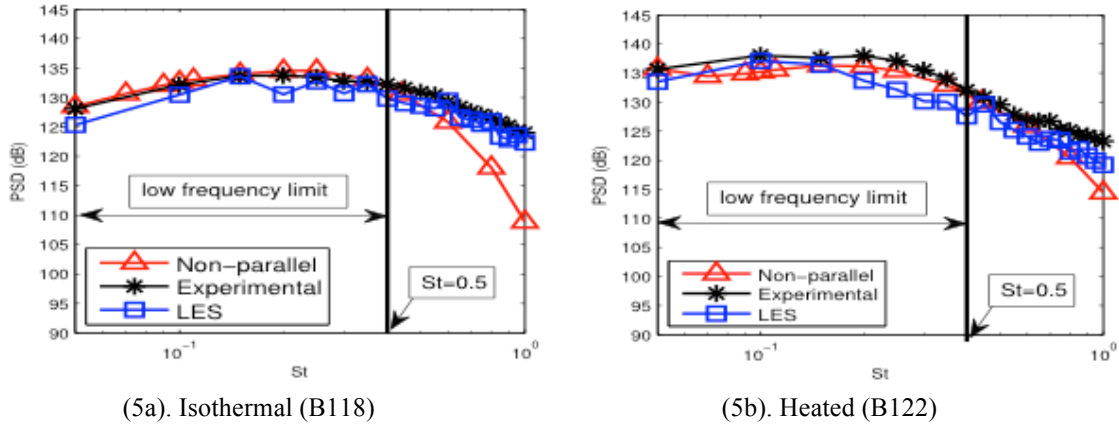


Figure 5. 30° spectrum predictions at $|x| = 100D_j$ corresponding to the experiment by Schlinker *et al.* [15] and LES predictions obtained from Brès *et al.* [12] & [13]

Note that when the same set of parameters are used for larger angles ($\theta = 45, 60$ deg), the acoustic spectrum predictions (shown in Figure 6 on right hand inset) are no longer in agreement, but this is not surprising since the model in its current form is supposed to provide accurate predictions at small observation angles and does not include auto-variances and co-variances associated with enthalpy flux and momentum flux/enthalpy flux coupling, respectively [8].

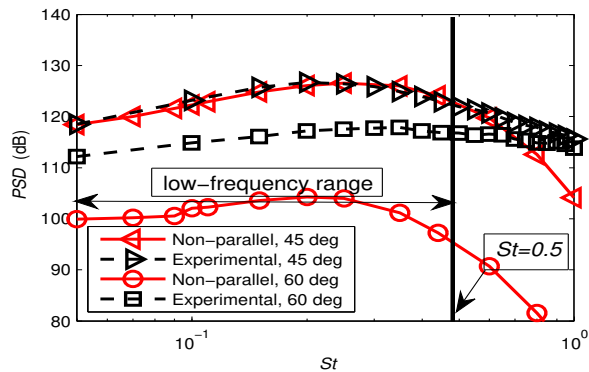


Figure 6. Breakdown of predictions at larger angles (same conditions at Fig. 5)

VI. PROPAGATOR SOLUTION FOR $O(1)$ STROUHAL NUMBERS

Since Afsar *et al.* [11] show that, for the round jet, the propagator tensor (5) expands as:

$$\Gamma_{ij}(\mathbf{y} | \mathbf{x}; \omega) = \delta_{i1} \delta_{j2} \Gamma_{1r}^{(0)}(\mathbf{y} | \mathbf{x}; \omega) + O(\varepsilon) = \begin{pmatrix} O(\varepsilon) & O(1) & O(\varepsilon) \\ O(\varepsilon) & O(\varepsilon) & O(\varepsilon) \\ O(\varepsilon) & O(\varepsilon) & O(\varepsilon) \end{pmatrix} + \dots \quad (22)$$

where suffix 2 is along radial direction and $\Gamma_{1r}^{(0)}(Y, r | \mathbf{x}; \omega) = \partial G_1^{(0)}(Y, r) / \partial r$ (and $\Gamma_{1r}^{(0)}(Y, r | \mathbf{x}; \omega) = \tilde{\Gamma}_{1r}(Y, U(Y, r) | \mathbf{x}; \omega)$ by the implicit function theorem where $\tilde{G}_i(Y, U(Y, r)) = G_i^{(0)}(Y, r)$ and where the superscript '(0)' refers to the lowest order azimuthal mode expansion). As mentioned earlier, this approximation is well confirmed by the numerical experiments conducted by G&L & Afsar (2010) on a parallel mean flow and Karabasov *et al.* (2010) on the full numerical solution to the adjoint Green's function equations (here written as (7) - (9)) all of which corroborate the asymptotic expansion (22) in that the $\Phi_{1r}^*(\mathbf{y}, \mathbf{k}, \omega)$ contracted with $|G_{1r}|^2$ in (12) dominates the small angle acoustic radiation. At higher frequencies, however, non-parallelism is sub-dominant in the leading order propagator solution and the dipole radiation induced by $\tilde{\Gamma}_{1r}(Y, U(Y, r) | \mathbf{x}; \omega)$ in the acoustic spectrum (12) may be approximated by a solution based on a locally parallel flow. This assertion can be easily confirmed by taking the limit $\Omega \rightarrow \infty$ (with spread rate fixed at $\varepsilon = O(1)$) in the leading order inner equation (18). An obvious distinguished limit for the leading order solution is one in which the streamwise variable is re-scaled into a region inasmuch as $Y = \Omega^{-1} \bar{Y}$ where $\bar{Y} = O(1)$ (GSA, p. 221). After changing variables in (18), it is immediately clear that the non-parallel flow term is asymptotically small (i.e. $O(\Omega^{-1})$) in this limit. There is ample numerical confirmation of the sub-dominance of non-parallel flow effect in the $\Omega \rightarrow \infty$ limit. See, for example, Fig. 16a in Karabasov *et al.* (2010) where the acoustic analogy prediction based on a locally parallel flow Green's function solution is identical to the full numerical calculation of the adjoint equations for frequencies greater than 1000 Hz (i.e. for Strouhal numbers > 0.1 , the peak frequency); moreover, in Fig. 16b of Karabasov *et al.* (2011), this overlap occurs at a later frequency of about > 0.3 after re-scaling by 2π to be consistent with our definition of Strouhal number.

In the parallel flow limit, $U = U(r)$ and $\partial \tilde{v}_j / \partial y_j = 0$. Hence, $\tilde{X}_1 = 0$ and adjoint equations (7)-(9) reduce to (G&L, p.299):

$$-\frac{\tilde{D}G_1}{D\tau} - \frac{\tilde{\sim} \partial G_4}{c^2 \partial y_1} - \frac{\partial G_5}{\partial y_1} = 0 \quad (23)$$

$$-\frac{\tilde{D}G_i}{D\tau} + G_1 \frac{\partial U}{\partial y_i} - \frac{\tilde{\sim} \partial G_4}{c^2 \partial y_i} - \frac{\partial G_5}{\partial y_i} = 0, \quad i = (2, 3) \quad (24)$$

$$-\frac{\tilde{D}G_4}{D\tau} - \frac{\partial G_i}{\partial y_i} = \frac{1}{2\pi} \delta(\mathbf{x} - \mathbf{y}) \quad (25)$$

$$-\frac{\tilde{D}G_5}{D\tau} = 0 \quad (26)$$

where $\tilde{D}/D\tau \equiv i\omega + U \partial / \partial y_1$. Since the frequency is order-one (inasmuch as, $St = O(1)$), the domain of $G_\lambda(\mathbf{y} | \mathbf{x}; \omega)$ no longer separates out into inner and outer regions in r . But because \mathbf{x} is in the far-field (as $|\mathbf{x}| \rightarrow \infty$), the adjoint equations (24)-(26) are homogeneous in the jet (i.e., right hand side of (25) is zero) and have coefficients that depend on the uniform flow in the far-field region when the Dirac does exist. The latter (Helmholtz equation in

$G_4(\mathbf{y} | \mathbf{x}; \omega)$ can then be solved by standard methods (pp. 826-828 of Morse & Feshbach 1953) which we discuss briefly for completeness ([9]).

Taking the convective derivative of (24) and using $i = 1$ component of the adjoint momentum equation (24) shows that

$$-\frac{\tilde{D}^2 G_i}{D\tau^2} - \tilde{c}^2 \left[\frac{\partial U}{\partial y_i} \frac{\partial G_4}{\partial y_1} + \frac{\tilde{D}}{D\tau} \frac{\partial G_4}{\partial y_i} \right] - \left[\frac{\partial U}{\partial y_i} \frac{\partial G_5}{\partial y_1} + \frac{\tilde{D}}{D\tau} \frac{\partial G_5}{\partial y_i} \right] = 0, \quad i = (1, 2, 3) \quad (27)$$

But after inserting, $\tilde{D}/D\tau (\partial G_\lambda / \partial y_i) = \partial / \partial y_i (\tilde{D} G_\lambda / D\tau) - \partial U / \partial y_i (\partial G_\lambda / \partial y_1)$, it follows that,

$$-\frac{\tilde{D}^2 G_i}{D\tau^2} - \tilde{c}^2 \frac{\partial G_0}{\partial y_i} = 0, \quad i = (1, 2, 3) \quad (28)$$

where we used Eq. (26) to eliminate $G_5(\mathbf{y} | \mathbf{x}; \omega)$ and where we have put, $G_0 \equiv \tilde{D} G_4 / D\tau$. Since $G_\lambda(\mathbf{y} | \mathbf{x}; \omega)$ now depends on the streamwise co-ordinates through $x_1 - y_1$ when the mean flow is independent of the streamwise co-ordinate we can take Fourier transforms in the streamwise direction to give the following

$$(\omega - Uk)^2 \hat{G}_i - \tilde{c}^2 \frac{\partial \hat{G}_0}{\partial y_i} = 0, \quad i = (1, 2, 3) \quad (29)$$

$$-\hat{G}_0 - \frac{\partial \hat{G}_i}{\partial y_i} = \frac{1}{(2\pi)^2} \frac{\delta(R-r)\delta(\Psi-\psi)}{r} \quad (30)$$

where,

$$\hat{G}_\lambda(\mathbf{y}_T | \mathbf{x}_T; \omega, k) \equiv \frac{1}{2\pi} \int_{-\infty}^{\infty} e^{-ik(x_1 - y_1)} G_\lambda(x_1 - y_1, \mathbf{y}_T | \mathbf{x}_T; \omega) d(x_1 - y_1), \quad \lambda = 1, 2, \dots, 5 \quad (31)$$

We have taken liberties of using the gradient operator symbol, to refer to the Fourier transform of the same operator, namely: $\nabla = \{-ike_1 + e_r \partial / \partial r + e_\psi \partial / r \partial \psi\}$ where tensor suffixes, $i = (1, 2, 3)$ are components of the cylindrical polar co-ordinate space with 1 being the streamwise direction, 2, the radial and 3 the azimuthal angle. Eq. (26) shows that the space-time Green's function, $g_5(\mathbf{y}, \tau | \mathbf{x}, t)$ is purely convected, i.e., $g_5 = g_5(\tau - y_1/U)$, which after taking Fourier transforms in the streamwise direction shows that $-i(\omega - Uk)\hat{G}_5 = 0$ and therefore that $\hat{G}_5(r, \psi | R, \Psi; \omega, k)$ must be zero at all $(\omega, k) \neq 0$ other than at the critical layer where $(\omega - Uk) = 0$. Hence the field equations for $\hat{G}_\lambda(r, \psi | R, \Psi; \omega, k)$ reduce to solving the two independent equations ([9]):

$$(\omega - Uk)^2 \hat{G}_r - \tilde{c}^2 \frac{\partial \hat{G}_0}{\partial r} = 0, \quad i = (1, 2, 3) \quad (32)$$

$$\left[1 - \frac{\tilde{c}^2}{(\omega - Uk)^2} k^2 + \frac{1}{r^2} \frac{\tilde{c}^2}{(\omega - Uk)^2} \frac{\partial^2}{\partial \psi^2} \right] \hat{G}_0 + \frac{1}{r} \frac{\partial r \hat{G}_r}{\partial r} = - \frac{1}{(2\pi)^2} \frac{\delta(R-r)\delta(\Psi-\psi)}{r} \quad (33)$$

for $r = O(1)$.

When r is in the jet region, Eqs. (32) & (33) can be used to solve the Rayleigh equation for \hat{G}_0 (see G&L), however, as indicated in [9], it is advantageous to retain them as first order equations to avoid differentiating the LES mean flow which might possess small oscillations in regions where the grid density is sparse. Since $|\mathbf{x}| \rightarrow \infty$, variation of parameters (p. 826 of Morse & Feshbach, 1953) and the method of stationary phase shows that we may legitimately look for solutions in the jet of the form $A_m(\theta; \omega) \tilde{G}_0^{(m)}(r | \theta; \omega) \cos m(\Psi - \psi)$ with pre-factor identical to the outer-field Helmholtz equation solution (which the above equations reduce to after eliminating \hat{G}_i). Hence

$$G_0(\mathbf{y} | \mathbf{x}; \omega) \rightarrow \frac{k_\infty^2}{4\pi|\mathbf{x}|} e^{-ik_\infty(y_1 \cos \theta - |\mathbf{x}|)} \sum_{m=0}^{\infty} (-i)^m \varepsilon_m A_m(\theta; \omega) \tilde{G}_0^{(m)}(r, \theta; \omega) \cos m(\Psi - \psi) \quad (34)$$

where $\varepsilon_m = 1$ for $m = 0$ and $\varepsilon_m = 2$ for $m \geq 1$ and where we have made use of the Jacobi-Anger formula (Eq. 27 of Bateman 1953, Vol. II) to re-write the azimuthal dependence $e^{im(\Psi - \psi)}$ of the basic solutions to (32) & (33) a sum over positive modes, m .

Inserting Eq. (34) (and an equivalent formula for $\tilde{G}_r^{(m)}$) into adjoint equations (32) & (33) with Fourier transform of the gradient operator given by $\tilde{\nabla} = \{-ike_1 + e_r(\partial/\partial r + 1/r) - e_\psi im/r\}$ gives two independent ordinary differential equations for $\tilde{G}_0^{(m)}(r | \theta; \omega)$ and $\tilde{G}_r^{(m)}(r | \theta; \omega)$

$$\frac{d\tilde{G}_0^{(m)}}{dr} = \frac{k_\infty^2}{a_r^2} (1 - M(r) \cos \theta)^2 \tilde{G}_r^{(m)} \quad (35)$$

$$\frac{d\tilde{G}_r^{(m)}}{dr} = \left[\frac{a_r^2 \cos^2 \theta}{(1 - M(r) \cos \theta)^2} + \frac{a_r^2 (m/r)^2}{k_\infty^2 (1 - M(r) \cos \theta)^2} - 1 \right] \tilde{G}_0^{(m)} - \frac{\tilde{G}_r^{(m)}}{r} \quad (36)$$

which can be solved numerically by marching forward using Runge-Kutta integration (see Afsar 2009b). In the neighborhood around the regular singular point, $r = 0$, the mean flow is nearly constant and the homogeneous form of Rayleigh equation in $\tilde{G}_0^{(m)}(r | \theta; \omega)$ reduces to a Bessel equation $\tilde{G}_4^{(m)}(r | \theta; \omega)$; hence

$\tilde{G}_4^{(m)}(r | \theta; \omega) \rightarrow J_m(r) \sim r^m$ (Abramowitz & Stegun 1963, p.360; see also Tam & Auriault 1998). Hence the numerical integration of (35) & (36) can start with $\tilde{G}_0^{(m)}(r_{start} | \theta; \omega) \rightarrow i\omega(1 - M(r_{start}) \cos \theta) r_{start}^m$ and

$\tilde{G}_r^{(m)}(r_{start} | \theta; \omega) = \frac{i\omega}{(k_\infty^2/a_r^2)(1 - M(r_{start}) \cos \theta)} m r_{start}^{m-1}$ (using Eq. (35)). The constant $A_m(\theta; \omega)$ in (34) is then found

by patching it onto the outer (Helmholtz equation) solution:

$$G_0(\mathbf{y} | \mathbf{x}; \omega) = \frac{k_\infty^2}{4\pi|\mathbf{x}|} e^{-ik_\infty(y_1 \cos \theta - |\mathbf{x}|)} \sum_{m=0}^{\infty} (-i)^m \varepsilon_m \left[J_m(rk_\infty \sin \theta) + B_m(\theta; \omega) H_m^{(1)}(rk_\infty \sin \theta) \right] \cos m(\Psi - \psi) \quad (37)$$

at $r = r_{end}$ where $M(r_{end}) = 0$.

In Figure 7 we show contour of $|\tilde{G}_{1,r}(\mathbf{y}; \omega)|$ based on solution (34) for Strouhal numbers $St = 0.4$

and $St = 0.8$ (isothermal) B118 jet. Since the pre-factor of $|\tilde{G}_{1r}(\mathbf{y}; \omega)|$ is proportional to dU/dr , the initial shear layers are weighted more than the downstream region (consistent with contour plots 15 & 17 in GSA which are at observation angle, $\theta = 30^\circ$) for $\theta = 60^\circ$ chosen here to avoid the critical layer singularity which for B118 jet occurs at the far-field locations, $\theta \leq \cos^{-1}(1/1.5) \approx 49^\circ$.

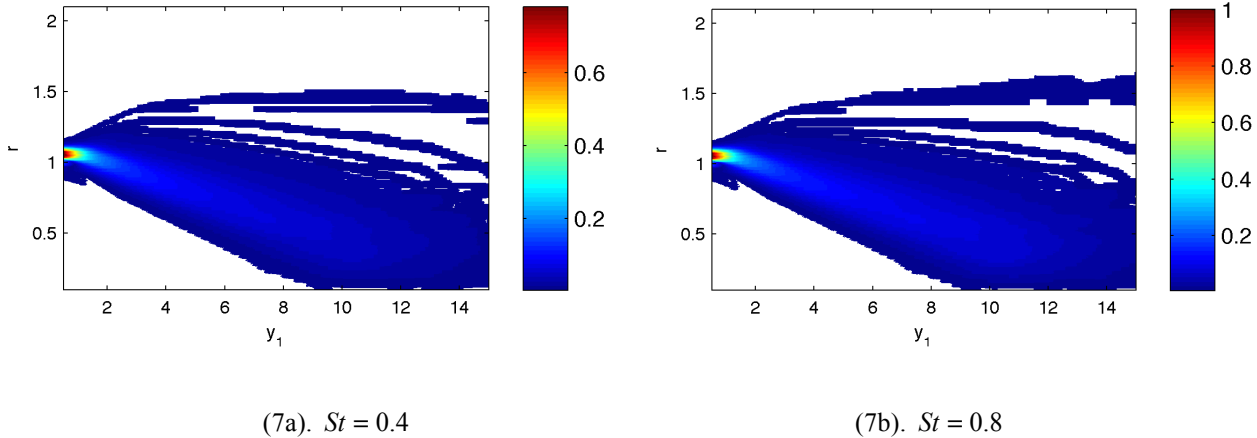


Figure 7. Contours of $|\tilde{G}_{1r}(\mathbf{y}; \omega)|$ based on locally parallel flow Green's function (34) for (isothermal) B118 jet

VI. CONCLUSIONS AND REMAINING ANALYSIS

This paper is a continuation of previous analysis (AIAA 2016-2804) in which an asymptotic solution to the adjoint Linearized Euler Equations (7)-(9) for the true non-parallel jet mean flow at low frequencies was used as a means for jet noise prediction under the distinguished limit in which mean flow spreading and rate of jet evolution are of same order. We have shown that this same approach (Eqs. (18)-(20)) provides a robust means of predicting supersonic jet noise up to Strouhal numbers of 0.6. Our aim is show that when this asymptotic solution is used together with the Rayleigh equation Green's function for a locally parallel mean flow at order-1 frequencies, the domain of the prediction model can be extended yet further. Towards this goal, we have solved and validated the solution to the latter and aim to use it within the acoustic spectrum formula, Eq. (4).

Acknowledgments

This work is a continuation of analysis presented at CTR Summer Program 2016 and the authors would like to thank Professor Parviz Moin for supporting us in that regard. MZA would like to thank Strathclyde University for financial support from the Chancellor's Fellowship. We warmly acknowledge Dr. Guillaume A. Brès (Cascade Technologies) for providing the LES database and, together with Prof. Joe Nichols (Univ. of Minnesota), helping with the initial analysis. We would also like to thank Dr. S. J. Leib (Ohio Aerospace Institute) for providing us with his spectral tensor routines and Dr. Aaron Towne (Stanford University) for useful discussions during the course of the Stanford Summer Program. The LES studies were supported by NAVAIR STTR project, under the supervision of Dr. John T. Spyropoulos. The main calculations were carried out at DoD HPCMP supercomputer facilities in ERDC DSRC.

REFERENCES

- [1]. Lighthill, M.J. 1952 On Sound Generated Aerodynamically: I. General Theory, *Proc. R. Soc. Lon.*, A 211, pp. 564–587.
- [2]. Goldstein, M. E. 2003. A generalized acoustic analogy. *J. Fluid Mech.* 488, pp. 315-333.
- [3]. Goldstein, M. E., Sescu, A. and Afsar, M.Z. 2012. Effect of non-parallel mean flow on the Green's function for predicting the low-frequency sound from turbulent air jets. *J. Fluid Mech.* 695, pp. 199-234.
- [4]. Karabasov, S. A., Bogey, C & Hynes, T. P. 2011 Computation of noise of initially laminar jets using a statistical approach for the acoustic analogy: application and discussion, AIAA 2011-2929, 17th AIAA/CEAS .
- [5]. Goldstein, M.E. and Leib, S.J. 2008, "The Aero-acoustics of slowly diverging supersonic jets," *J. Fluid Mech.*, 600, pp.291-337
- [6]. Crocco, L., 1932 Sulla transmission del calore da una lmina piana aun fluido scorrente ad alta velocita. L'Aerotenza, 12, pp. 181-197. Translated as NACA TM 690.
- [7]. Leesshafft, L., Huerre, P., Sagaut, P. & Terracol, M. 2006 Nonlinear global modes in hot jets. *J. Fluid Mech.* 554, 393–409.
- [8]. Afsar M. Z., Goldstein, M. E. & Fagan, A. M 2011 Enthalpy flux/Momentum flux Coupling in the Acoustic Spectrum of Heated Jets. AIAAJ, Vol. 49, No. 11, pp. 2522-2531.
- [9]. Afsar, M. Z. 2010 Asymptotic properties of the overall sound pressure level of sub-sonic air jets using isotropy as a paradigm. *J. Fluid Mech.* 664, 510–539
- [10]. Leib, S. J. & Goldstein, M. E. 2011 A Hybrid Source Model for Predicting High-Speed Jet Noise. AIAAJ, Vol. 49, No. 7, pp. 1324-1335.
- [11]. Afsar, M. Z., Sescu, A., & Leib, S. J. 2016 Predictive Capability of Low Frequency Jet Noise using an Asymptotic Theory for the Adjoint Vector Green's Function in Non-parallel Flow. AIAA 2016-2804.
- [12]. Brès, G. A., Nichols, J. W., Lele, S. K. and Ham, F. 2012 Towards Best Practices for Jet Noise Predictions with Unstructured Large Eddy Simulations. AIAA Paper 2012-2965.
- [13]. Brès, G.A., Ham, F.E., Nichols, J.W. & S.K. Lele, Unstructured Large Eddy Simulations of Supersonic Jets, accepted for publication in AIAA J., 2016.
- [14]. Afsar, M. Z., Sescu, A., Sassanis, V., Towne, A., Brès, G. A. and Lele, S.K. 2016/ Prediction of supersonic jet noise using non-parallel flow asymptotics and LES data within Goldstein's acoustic analogy. Proceedings of the *Center for Turbulence Research Proceedings of the Summer Program 2016* .
- [15]. Schlinker, R. H., Simonich, J. C., Reba, R. A., Colonus, T., Gudmundsson, K., & Ladeinde, F., Supersonic Jet Noise from Round and Chevron Nozzles: Experimental Studies, AIAA Paper 2009-3257, 2009.
- [16]. Abramowitz, M. and Stegun, I. A., 1965, *Handbook of Mathematical Functions*, National Bureau of Standards, Washington, DC.
- [17]. Bateman, H. 1954. *Table of Integral transforms Vol. II*. Bateman Manuscript Project, Chief Editor: Erdelyi, A. McGraw Hill Book Co., NY, USA.
- [18]. Morse, P. M. and Feshbach, H., 1953, *Methods of Theoretical Physics*, McGraw-Hill Book Company

- [19]. Karabasov, S.A., Afsar, M.Z., Hynes, T.P., Dowling, A.P., McMullan, W.A., Pokora, C.D., Page, G.J. and McGuirk, J.J.. "Jet Noise - Acoustic Analogy informed by Large Eddy Simulation". AIAA J, 48(7), pp. 1312-1325.